ISSN 2075-1133, Inorganic Materials: Applied Research, 2016, Vol. 7, No. 6, pp. 884–891. © Pleiades Publishing, Ltd., 2016.
Original Russian Text © G.N. Sokolov, V.I. Lysak, I.V. Zorin, A.A. Artem'ev, Yu.N. Dubtsov, V.O. Kharlamov, A.A. Antonov, 2015, published in Voprosy Materialovedeniya, 2015, No. 4(84), pp. 159–168.

Phenomenological Model of Crystallization Center Nucleation in Metal Melt during Welding under the Influence of Ultrafine Refractory Components

G. N. Sokolov*, V. I. Lysak, I. V. Zorin, A. A. Artem'ev, Yu. N. Dubtsov, V. O. Kharlamov, and A. A. Antonov

**e-mail: gnsokolov@yandex.ru*

Received September 8, 2015

Abstract—Metallography reveals the correlations between the amount, size, and morphology of ultrafine particles in welding materials (flux-cored and composite wires, coated electrodes, and agglomerated fluxes), as well as the processes of formation of exogenous crystallization centers in the welding pool that facilitate the structure modification and promotion of processing and working properties of deposited metal. The phenomenological model of the nucleation on ultrafine exogenous refractory chemical clusters is developed on the basis of the experimental data and on the existing view of the kinetics of fast physicochemical processes in the welding fire point.

Keywords: heat- and wear-resistant alloys, refractory chemical compounds, exogenous modifier, crystallization centers, model

DOI: 10.1134/S2075113316060204

INTRODUCTION

In technological surfacing characterized by powerful thermal and dynamic influence of sources of heat on the metal melt, it is rather difficult to control the transition of ultrafine refractory components (UFRCs) in the weld metal, which are injected in the reactive zone in various welding materials for purposeful formation of its structure, as well as the welding and technological properties. This favors the relevance of novel scientific and engineering solutions in the alloying of heat- and wear-resistant weld alloys with refractory particles.

Summarizing the experience of nanostructuring of surface layers for structural and instrumentation materials, the authors [1] mentioned a lack of technologies to create a large-volume homogeneous nanostructure, as well as the difficulty of its formation in welding compounds. It was also shown that the embedding of UFRCs with nanoparticles in the welding bath refines the structure of the weld metal [2, 3] and welds [4, 5] with the improvement of their mechanical and operational properties. Despite the fact that the studies in this field of research were further developed [6–11], the mechanisms of formation of a structure providing a high-strength state in the weld metal under the effect of UFRCs are not yet elucidated.

This work is thus aimed at establishing the mechanism of crystallization center nucleation of heat- and wear-resistant weld metal through the introduction of UFRCs.

METHODS OF CHARACTERIZATION OF STRUCTURE AND PROPERTIES OF THE WELD METAL

The structure, chemical composition, and micromorphology of the weld metal were examined on the optical Carl Zeiss Axiovert 40 MAT digital microscope and FEI Versa 3D scanning two-beam electron ion microscope. The micro-X-ray spectral analysis was performed on an Apollo X energy dispersion silicon-lithium spectrometer. The cross-section profiles of the weld metal were prepared by means of etching via the focusing of a Ga^+ ion beam with energy of 30 kV. Before etching, the surface section was covered with a thin platinum layer in order to prevent cross-section surface damage by the ion beam.

The thermal force resistance of the weld metal was estimated from the sclerometric tests of samples over the temperature range of 750–1250°C in accordance with the technique developed on the basis of scanning probe microscopy with use of a Solver Pro microscope (RF patents nos. 2281575 and 87018) by measuring the cross-section profile parameters and calculating the deformed metal volumes (Rockwell indenter) on a segment 10 mm long. The shock viscosity of welds at negative temperatures on the Celsius scale was evalu-

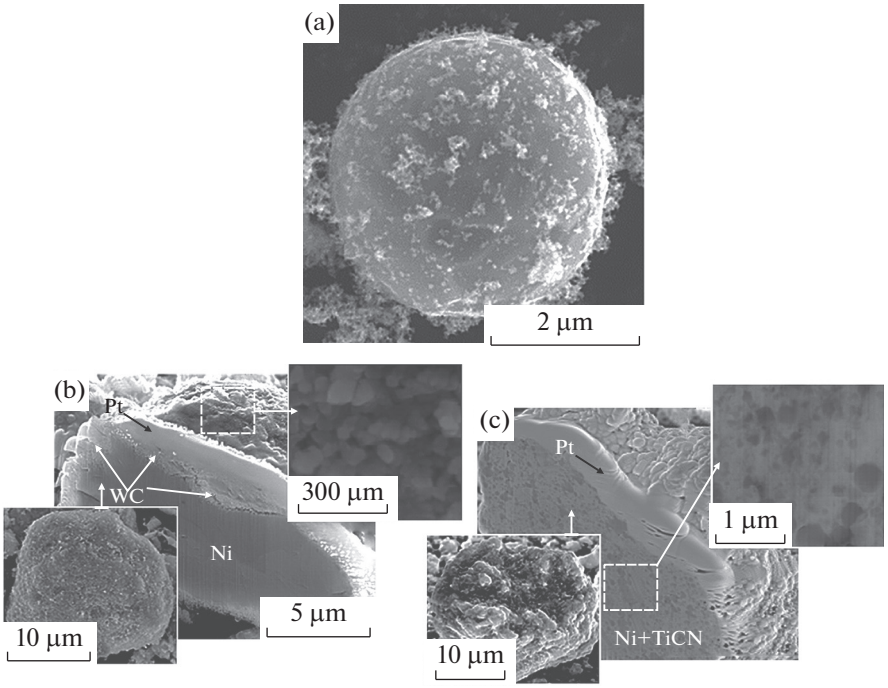

Fig. 1. Image of a TiN titanium nitride granule with TiN nanoparticles at the surface (a), nickel granules with incorporated WC tungsten carbide particles (b) and TiCN titanium carbonitride (c). Pt is the platinum layer applied with the ion beam.

ated in agreement with GOST 9454-78. The abrasive wear resistance was determined at a load of 0.937 MPa (GOST 17367–71) and its attrition with sandpaper of abrasive grit of P100. The weight losses of samples during the tests were estimated with the accuracy of 0.1 mg using annealed steel 45 as the reference. The thermal fatigue crack resistance of weld metals was evaluated upon the heating of samples to 1000°C and during the subsequent cooling in tap water to 50°C. The duration of the heating–cooling cycle was 1 min. The criterion of the thermal resistance was the number of cycles until the emergence of cracks observed in a fourfold optical zoom.

APPLIED MATERIALS AND EXPERIMENT

Mixed nano- and microscale TiN nitride powders with fractional composition (50 nm–5 μm) served as UFRCs. Spherical microparticles form conglomerates with nanoparticles which possess high surface energy (Fig. 1a), which favors their homogeneous distribution in the modifier introduced into the filler.

Nickel microgranules with the dimensions to 50 μm were used as the modifying components, which were alloyed with 30 wt % of WC carbide and TiCN carbonitride particles with sizes of 40–60 and 80–100 nm, respectively (Figs. 1b and 1c).

Modifiers with titanium nitride and nickel microgranules were introduced into the surface layer of bilayer coatings of the main-type electrodes with a diameter of 3 mm. They were also placed in the fillers of powder (with the diameters of 2.5 and 3 mm) and composite (3-mm-diameter) wires, as well as in the agglomerate flux granules with the CaF_2–Al_2O_3–CaO gas system (RF patents nos. 2407617, 2446930, 2471601, 2478029, and 2478030) (Fig. 1b).

The weld metal samples were prepared via multistage arc welding with a consumable electrode in argon, ESW with the CaF_2–Al_2O_3–CaO–SiO_2 flux system, and automatic welding with Sv-08A wire under the agglomerated flux and the DC manual arc welding (the positive electrode). The studied types of weld alloys are presented in the table.

RESULTS AND DISCUSSION

Metallography has revealed that the alloying of weld metal with TiCN carbonitride (table, alloy 1) reduces its grain size by more than a factor of two (from 25–35 to 8–10 μm). Moreover, the dopant elements are redistributed in γ-solid solution dendrites with the formation of homogeneously located low-carbon rack-type martensite inclusions therein.

The predominately disperse intermetallic spherical particles (0.5–1.5 μm, Fig. 2) composed of the most refractory elements (chromium, molybdenum, and manganese) were formed in the axial bulks of dendrites. They are surrounded by an intermediate zone, and multiple TiCN particles with the dimensions of 5 to 20 nm (presumably over several hundred) are

Type and structure of the studied alloys

Alloy no.	Type of weld metal	Welding method	Structure of weld metal	UFRC, wire, flux and electrode content, wt %
1	09Kh15N4AM3T	Arc welding in argon with flux-cored wire	Metastable austenite, martensite, intermetallides	0.4 TiCN
2	10Kh4N74Yu10M3V5TT Tantalum content (TT) 3 wt %		$\gamma + \gamma'$ doped solid solution (Ni_3Al)	0.25 WC
3	400Kh13M2T2NR		Carboboride eutectic, iron, iron-chromium carboborides, titanium nitrides, double titanium and molybdenum carbides	0.6 TiN
4	200Kh10N4 + 25% TiB_2	ESW with flux-cored wire additive	Carboboride eutectic, TiB_2 inclusions, titanium carbides, iron-chromium carboborides and borides	0.6 TiCN
5	12GS	MAW with covered electrode	Carbides, borides, carboborides	3.0 (WC + Ni)
6	09GSN	Arc welding under flux	Ferrite and perlite	1.5 (WC + Ni)

detected in their sections with the ion beam. In metallic melt, there can also be the interaction between the nanoparticle clusters with surface active sulfur [10], but its identification at the sections with sizes less than 500 nm is difficult because of the superposed Lα and Kα energy spectra from the sulfur and molybdenum atoms, respectively. These structural and phase transformations caused a twofold increase in the deformation resistance of weld metal at temperatures up to 900°C (Fig. 3a).

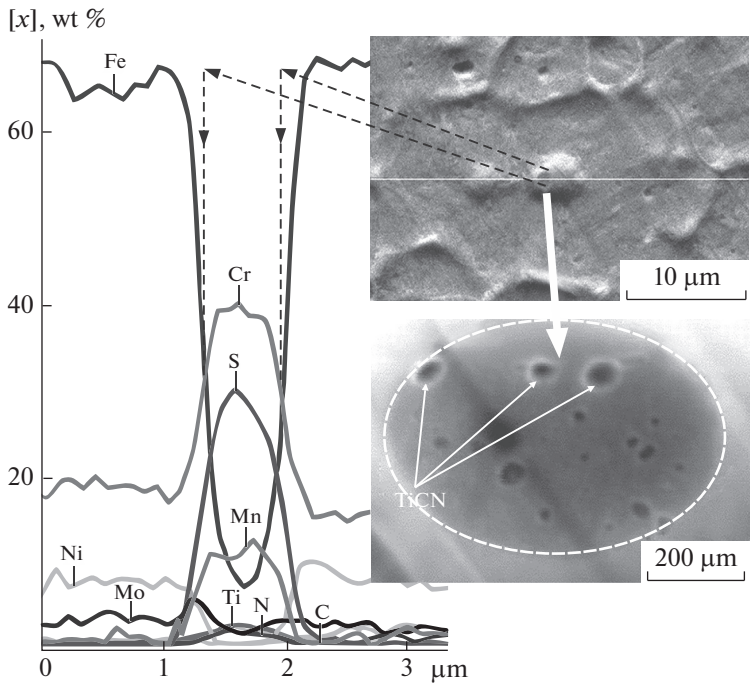

Fig. 2. Intermetallic compounds at the central part of grain of austenite-martensite metal weld with use of TiCN nanoparticles (alloy 1).

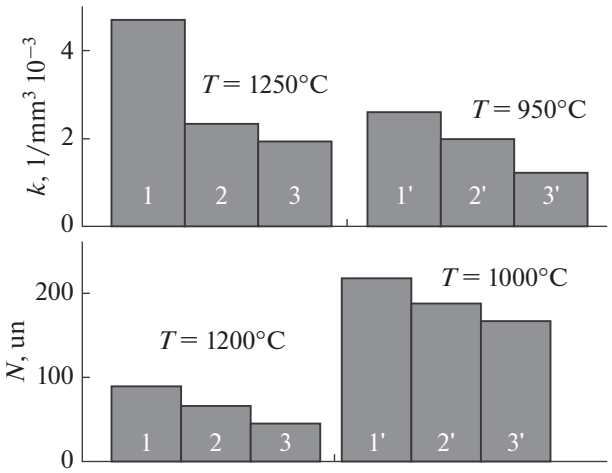

Fig. 3. (a) Parameter k characterizing the plastic deformation resistance of weld metal and (b) number of cycles N until the emergence of the first crack during thermal fatigue tests: (*1*, *1'*) 10Kh4N74Yu10M3V5TT (alloy 2) and 09Kh15N4AM3T (alloy 1) with UFRC; (*2*, *2'*) the same alloys welded without UFRC; (*3*, *3'*) industrial 02Kh15N65M16V4 and DN-S WA (03Kh13N5K2AMVFSG) alloys.

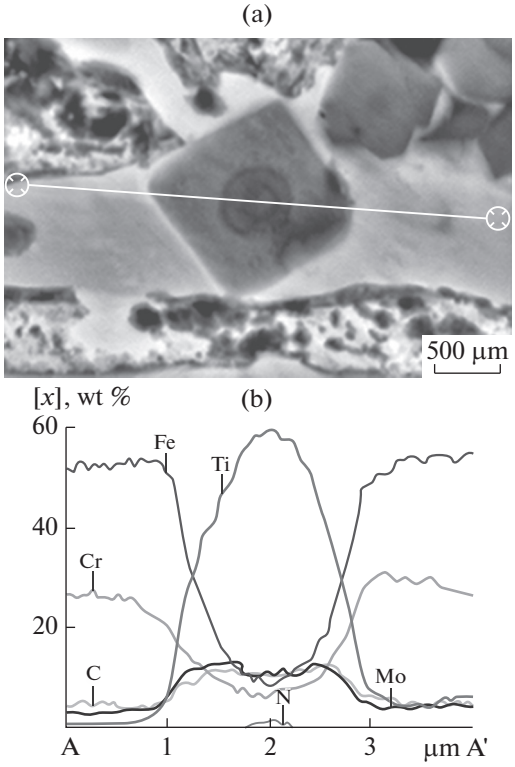

Fig. 4. (Ti, Mo)C_{1-x} carbide in alloy 3 welded with use of TiN nanoparticles.

The examination of wear-resistant weld metal of the Fe–Cr–Mo–Ni–Ti–C–B system (table, steel 2) doped with titanium nitride micro- and nanoparticles enabled us to establish the dispersion of $(Fe, Cr)_7(C, B)_3$ carboborides under the action of TiN particles with an augmenting amount of small (1–3 μm) (Ti, Mo)C_{1-x} cubically shaped carbides which are the solid solution of isostructural TiC and MoC_{1-x} carbides [11]. There are circularly and cubically shaped inclusions with the sizes of 300–800 nm at the centers of the sections in these carbides (Fig. 4), and the circular inclusions are surrounded by a visible transition band with the width of 100–150 nm. The analysis of the chemical composition of inclusions revealed a high titanium content and nitrogen therein independently of their morphology (Fig. 4). Evidently, the circularly shaped TiN particles partially dissolved and transferred from the modifier in the metal melt, as well as the cubic TiN particles released, become the crystallization centers of (Ti, Mo)C_{1-x} carbides. As was found, the structural changes in the metal was due to the increase in its hardness by 8%, as well as to the increase in abrasive wear resistance by 12% at 500°C.

The characterization of the abrasive wear resistant Fe–Cr–Mo–Ni–Ti–C–B alloy reinforced with TiB_2 microparticles shows that the injection of TiCN nanoparticles causes a release of numerous ultrafine (0.8–6 μm) titanium compounds (TiC, TiN, and TiCN) in the metal, which are homogeneously distributed in its matrix. There is also a decrease in the sizes and microhardness (from 22 to 17 MPa) of coarsened iron-chromium borides and carboboride crystals. The circular inclusions with size of 70 to 250 nm with a high amount of calcium were also detected in the sections of TiC particles (Fig. 5). They can be assumed to be the TiCN–$CaTiO_3$ complexes formed in the interaction of TiCN particles in the metal melt with the calcium and oxygen ions which are the surface active CaF_2–Al_2O_3–CaO–SiO_2 slag system. They serve as the nuclei in the melt, being the crystallization centers for TiC carbides upon cooling. Severe microstructural changes in the melt favor a slight increase in its hardness (from 51 to 53 HRC), as well as a twofold increase in its abrasive wear resistance at room temperature.

The TEM scanning of 85-nm-thick nickel aluminide weld metal samples doped with WC nanocarbide (table, alloy 3) revealed particles with size of 200–270 nm in the bulk of γ' phases whose composition is close to eutectic, where the content of refractory elements (tungsten, molybdenum and tantalum) is much higher than in the remaining volume of the γ' phase compared to the γ-phase composition (Fig. 6). Their origin can be caused by the presence of WC tungsten carbide nanoparticles in the melt of the welding bath, which serve as the crystallization centers for refractory elements forming the intermetallic compound surrounded by Ni_3Al. This process is accompanied by the change in the alloy microstructure [10], which favors an increase in its plastic deformation resistance by 1.5–2 times at a temperature of 1200°C (Fig. 3).

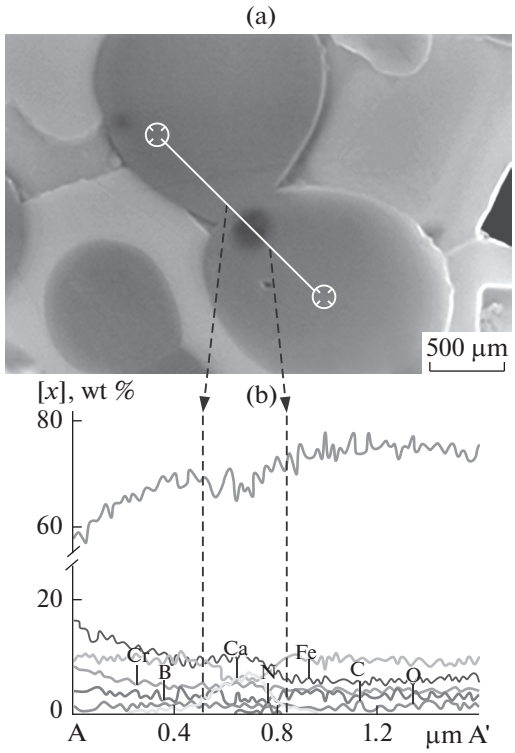

Fig. 5. TiC carbide in alloy 4 and distribution of dopants.

The effect of WC carbide and nickel nanoparticles in the electrode coatings and agglomerated flux on the structure and brittle fracture resistance of the weld metal (table, alloys 5 and 6) at a temperature of –60°C was manifested in the refinement of the initial ferrite–perlite structure (the grain size of 8 to 13 points) with the formation of low-bainite domains therein (Fig. 7), which led to an almost 50% increase in the shock viscosity of the weld metal.

Analyzing the results, one can summarize that the influence of nano- and microscale refractory chemical compounds in UFRCs on the crystallization center nucleation in doped metal melt is different. The mechanism of crystallization centers formed around each particle with sizes of several hundred nanometers to several microns is known [12–14] and takes place in weld alloys 3 and 4 (table). The effect of particles smaller than 100 nm is not yet clear and it can be considered in the context of the phenomenological model based on the experimental data confirming the nucleation of crystallization centers in doped metal melt, which are formed at the clusters of refractory chemical compound nanoparticles.

As was shown [15], the transition of refractory nanoparticles from the modifier to the metal melt of a droplet begins during the heating of the welding electrode by the passage of current, as well as by the active spot of the electric arc. In this case, there is the formation of a heterogeneous metal–slag layer with the solid exogenous phase at a narrow area near the melting front between the electrode material and the metal melt (Fig. 7), which coincides with the data [16].

Upon the melting of the electrode material at the nucleation stage and the growth of metal droplets,

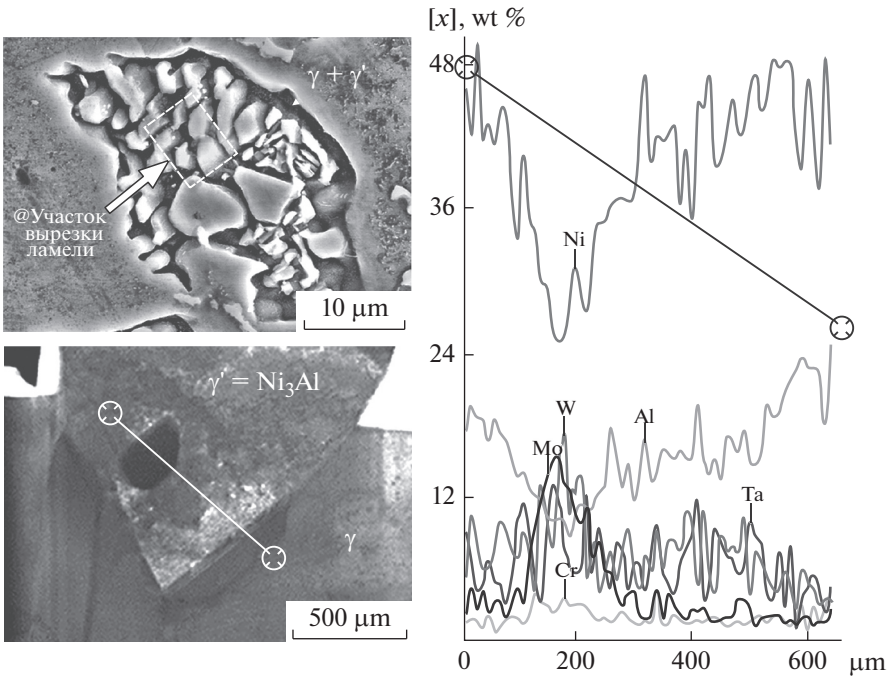

Fig. 6. Localization of γ' phases formed from γ-solid solution in weld alloy 2 and distribution of dopants in the bulk of γ' phase.

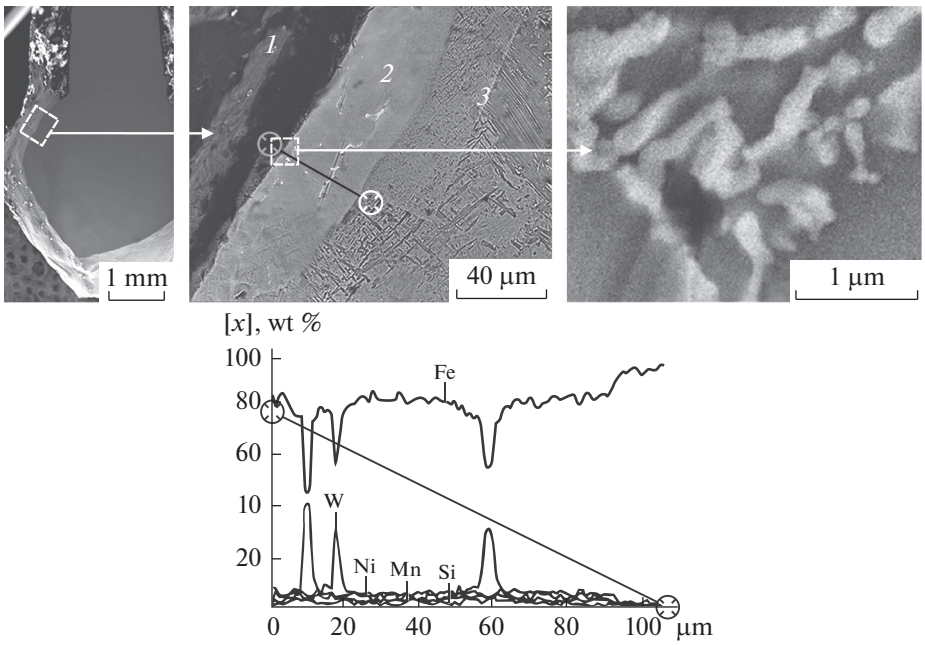

Fig. 7. Structure of characteristic area of metal crystallized near the melting front of the electrode side and the dopant element distribution therein: (*1*) slag layer at the droplet surface; (*2*) layer with the exogenous solid phase; (*3*) droplet metal.

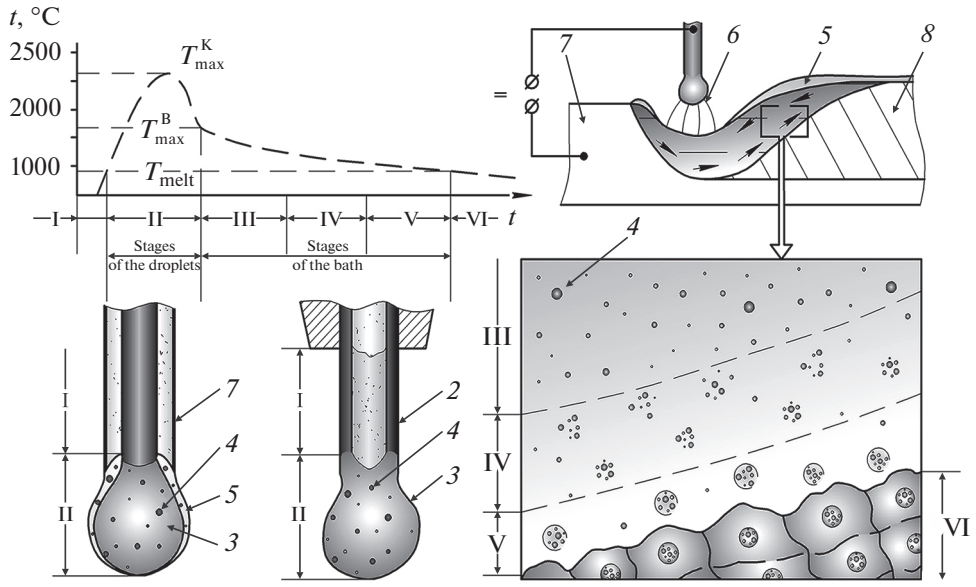

Fig. 8. Phenomenological model of modification of weld alloys with use of refractory compounds by example of arc welding with a covered electrode and flux-cored wire: (*1*) electrode with bilayer coating; (*2*) flux-cored wire; (*3*) molten metal droplet; (*4*) refractory compound nanoparticles; (*5*) slag; (*6*) electric arc; (*7*) basic metal; (*8*) weld metal; (*I*–*VI*) stages of the process; (→) direction of metal molten flux; (T^{K}_{max}, T^{B}_{max}) maximum temperatures of metal molten droplets and bath; (T_{melt}) melting point of metal; (*t*) time.

nanoparticles in the carrier component transporting them (nickel, complex modifier, or other objects) and in the free state pass into the metal melt superheated to 2100–2300°C and into the slag phase (Fig. 8). The metallurgical treatment reduces the content of atmospheric gas introduced with the nanoparticles with the subsequent activation of their surface and the partial dissociation of the finest fraction [17].

In the low-temperature (below 2000°C) slag melt contacting the metal droplets, as well as in that passing

with them into a reactive welding zone, the probability of dissociation of refractory nanoparticles is minimal, but they can redistribute between the slag and metal phases at this stage. When transiting into the metal of a welding bath, the nanoparticles adsorb the surface active elements—oxygen and sulfur or chemical compounds on their basis—onto their surface. The nanoparticle–surface active substance complexes are homogeneously distributed in the metal melt, forming with it the suspension, where the solid particle transfer is described by the known Zhukhovitskii formula [18]. The movement of this suspension in the peripheral zone of the welding bath removed from the heat source causes the conditions for a periodic decrease in the metal flux rate [19–21], which favors its supercooling in combination with other factors. In the cooled metal melt layer, the nanoparticle–surface active substance complexes are formed into clusters, which attract the diffusion of the most refractory dopant metal elements, leading to the formation of multiple segregations with sizes of 500–1500 nm. Besides the wave structure of molten dendrites periodically formed at the crystallization front [22], these segregations serve as additional centers for the nucleation of crystallites, favoring the exogenous modification of the weld metal.

CONCLUSIONS

The physicochemical processes taking place in the interaction of the modifier containing ultra- and nanoscale particles of refractory chemical compounds with the metal melt upon the melting of weld materials, droplet transfer, and formation of weld metal layers cause the partial dissolution of refractory particles, which can merge into clusters. The remaining particles or their clusters become the crystallization centers for dispersed reinforcing phases with the most refractory dopant elements in this alloying system.

ACKNOWLEDGMENTS

This work was supported by the Russian Foundation for Basic Research (project no. 14-08-00868) and by the grant of the President of the Russian Federation no. MK-4265.2014.8.

REFERENCES

1. Panin, V.E., Sergeev, V.P., Panin, A.V., and Pochivalov, Yu.I., Nanostructuring of surface layers and production of nanostructured coatings as an effective method of strengthening modern structural and tool materials, *Phys. Met. Metallogr.*, 2007, vol. 104, no. 6, pp. 627–636.
2. Ryabtsev, I.A., Kondrat'ev, I.A., Gadzyra, N.F., et al., Influence of ultrafine carbides in the flux-cored wire on the properties of heat-resistant welded metal, *Avtom. Svarka*, 2009, no. 6, pp. 13–16.
3. Sokolov, G.N., Lysak, V.I., Troshkov, A.S., et al., Modifying of weld metal by nanosized tungsten carbides, *Fiz. Khim. Obrab. Mater.*, 2009, no. 6, pp. 41–47.
4. Eremin, E.N., The use of nanoparticles of refractory compounds to improve the quality of welded joints of superalloys, *Omsk. Nauch. Vestn.*, 2009, no. 3, pp. 63–67.
5. Golovin, E.D., Bataev, A.A., Cherepanov, A.N., and Bolotova, L.K., Application of nanopowders of refractory compounds in the laser welding of carbon steels, *Ross. Nanotekhnol.*, 2009, vol. 2, nos. 3–4, pp. 35–57.
6. Hou, Q.V., Huang, Z., and Wang, J.N., Influence of nano-Al_2O_3 particles on the microstructure and wear resistance of the nickel-based alloy coating deposited by plasma transferred arc overlay welding, *Surf. Coat. Technol.*, 2011, vol. 206, nos. 8–9, pp. 2806–2812.
7. Artemyev, A.A., Sokolov, G.N., and Lysak, V.I., Effect of microparticles of titanium diboride and nanoparticles of titanium carbonitride on the structure and properties of deposited metal, *Met. Sci. Heat Treat.*, 2012, vol. 53, no. 11, pp. 603–607.
8. Smirnov, A.N., Knyaz'kov, V.L., Radchenko, M.V., et al., Influence of nano-dispersed particles of Al_2O_3 on the structural-phase state of coating systems Ni–Cr–B–Si/WC obtained by plasma-powder surfacing, *Svarka Diagn.*, 2012, no. 5, pp. 32–37.
9. Kobernik, N.V., Chernyshov, G.G., Gvozdev, P.P., et al., Antifriction properties of the coatings obtained by plasma welding of babbitt with carbon nanotubes, *Svarka Diagn.*, 2013, no. 3, pp. 27–31.
10. Sokolov, G.N., Zorin, I.V., Artem'ev, A.A., Litvinenko-Ar'kov, V.B., Dubtsov, Yu.N., Lysak, V.I., Kharlamov, V.O., Samokhin, A.V., and Tsvetkov, Yu.V., Structure formation and properties of weld alloys with addition of refractory compound nanoparticles, *Inorg. Mater.: Appl. Res.*, 2015, vol. 6, no. 3, pp. 240–248.
11. Zhilyaev, V.A., Fedorenko, V.V., and Shveikin, G.P., The mechanism of forming of the coaxial structure in alloys based on carbide and titanium carbide, *Tr. V mezhd. konf. po poroshkovoi metallurgii v Chekhoslovatskoi Sotsialisticheksoi Respublike* (Proc. V Int. Conf. on Powder Metallurgy in Czechoslovakia Social Republic), Gottwaldov, 1978, vol. 2, pp. 189–200.
12. Mal'tsev, M.V., *Modifitsirovanie struktury metallov i splavov* (Modification of the Structure of Metals and Alloys), Moscow: Metallurgiya, 1964.
13. Rebinder, P.A., *Izbrannye trudy. Kniga 2. Poverkhnostnye yavleniya v dispersnykh sistemakh. Fiziko-khimicheskaya mekhanika* (Selected Research Works, Book 2: Surface Processes in Dispersed Systems. Physical-Chemical Mechanics), Moscow: Nauka, 1979.
14. Saburov, V.P., Eremin, E.N., Cherepanov, A.N., et al., *Modifitsirovanie stalei i splavov dispersnymi inokulyatami* (Modification of Steels and Alloys by Dispersed Inoculators), *Omsk*: Omsk. Gos. Tekh. Univ., 2002.
15. Sokolov, G.N., Lysak, V.I., Zorin, I.V., Artem'ev, A.A., Dubtsov, Yu.N., and Troshkov, A.S., Effect of ultrafine components on welded joint metal properties for metal

structure operation at negative temperatures, *Chem. Petrol. Eng.*, 2015, vol. 51, no. 3, pp. 286–290.

16. Erokhin, A.A., *Osnovy svarki plavleniem. Fiziko-khimicheskie zakonomernosti* (Fundamentals of Fusion Welding: Physical-Chemical Principles), Moscow: Mashinostroenie, 1973.
17. Grigorov, I.G. and Zainulin, Yu.G., Dependence of melting temperature of nanodispersed titanium carbonitride from particle radius, *Perspekt. Mater.*, 2007, no. 6, pp. 60–63.
18. Zhukhovitskii, A.A., Belashchenko, D.K., and Bekshtein, B.S., *Fiziko-khimicheskie osnovy metallurgicheskikh protsessov* (Physical-Chemical Principles of Metallurgical Processes), Moscow: Metallurgiya, 1973.
19. Woods, R. and Milner, D., Motion in the weld pool in arc welding, *Weld. J.*, 1971, no. 4, pp. 163–173.
20. Erygin, V.I., Analysis of melt movement rate in the rear of the bath during welding by consumable electrode, *Svarochnoe Proizvod.*, 1980, no. 3, pp. 3–5.
21. Stolbov, V.I., *Svarochnaya vanna: monografiya* (Welding Bath: Monograph), Tolyatti: Toliat. Gos. Univ., 2007.
22. Shneerson, V.Ya., The formation of the layered structure of the weld metal during welding fusion, *Svarka Diagn.*, 2013, no. 4, pp. 16–23.

Translated by O. Maslova

SPELL: 1. OK